ASSESSMENT OF COUPLED LAGRANGIAN–EULERIAN FINITE ELEMENT SIMULATIONS TO MODEL SUCTION FORCES DURING HYDRODYNAMIC IMPACTS

MATHIEU GORON[1,2], BERTRAND LANGRAND[1,3], THOMAS FOUREST[1],
NICOLAS JACQUES[2] & ALAN TASSIN[4]
[1]DMAS, ONERA, France
[2]ENSTA Bretagne, France
[3]University Polytechnique Hauts-de-France, France
[4]IFREMER, France

ABSTRACT

During the emergency landing of an aircraft on water, the structure may experience critical forces and could eventually fail. The appropriate design of the structure should minimize the risk of occupant injuries. The recent progress in computation capabilities led to the increased use of numerical simulations in the certification process of aircraft. A specific challenge concerns the modelisation of suction forces that develop near the aircraft tail, where the first contact with water occurs. This phenomenon is due to the high horizontal velocity of the structure at impact and the longitudinal curvature of the fuselage. It can affect the overall aircraft kinematics during ditching. In this work, as an effort to improve aircraft ditching simulations and to assess the capabilities of numerical models to describe suction forces, the simple test case of the wedge water entry and subsequent exit is considered. Numerical simulations with the Eulerian formulation for the fluid and the Lagrangian formulation for the structure are used. The method used for the fluid–structure interaction is based on an immersed contact interface with penalty forces. The present work focuses on impact and suction forces modelling. Results show a satisfying capacity of the numerical approach to model negative hydrodynamic force (suction).

Keywords: finite elements, fluid–structure interaction, Eulerian–Lagrangian coupling, water impact and exit, hydrodynamic forces, suction.

1 INTRODUCTION

A hydrodynamic impact is a contact between a structure and a fluid in relative motion. The study of this phenomenon is motivated by various applications such as hull slamming, spacecraft (capsule), aircraft and rotorcraft emergency water landing (ditching). The hydrodynamic forces caused by water impacts are critical and considered during the sizing and certification of structures exposed to this kind of event.

The physical phenomena encountered during hydrodynamic impacts are well known for "ideal" impact conditions: vertical impact, simple geometry, rigid structure, fluid initially at rest, impact velocity large enough to neglect gravity, etc. Analytical approaches, mainly based on von Karman's [1] or Wagner's [2] theories, have been developed to analyse the loading applied to the structure. Numerous articles can be found in the literature, addressing the problem of hydrodynamic impact of simple geometries experimentally (wedges [3]–[5], circular cylinders [6], [7], cones [8], flat plates [9], spheres [10]) and numerically [11]–[14]. The recent advances in numerical simulation have gradually allowed the study of more complex phenomena (considering certain non-linearities related to the fluid–structure interaction, complex geometries, etc.), representative of realistic industrial applications. The finite element (FE) method, with a Lagrangian framework, is usually used to model the structure. The fluid behaviour can be described by various methods: Lagrangian [15],

WIT Transactions on The Built Environment, Vol 209, © 2022 WIT Press
www.witpress.com, ISSN 1743-3509 (on-line)
doi:10.2495/HPSU220101

Eulerian [16], [17], arbitrary Lagrangian–Eulerian (ALE) [18], or mesh-free methods such as smoothed particle hydrodynamics (SPH) [16].

The physical phenomena encountered during realistic industrial applications are more complex. For instance, during high-velocity oblique impacts suction, cavitation, ventilation, aeration or flow separation phenomena can appear and incapacitate the existing analytical and numerical approaches. Using these approaches in a sizing or certification context is therefore difficult at the moment as they require further developments.

In the present work, the explicit FE solver Radioss is used. A coupled Eulerian–Lagrangian (CEL) approach is considered to model ditching or water impact problems. On the one hand, the structure is described by a Lagrangian approach. On the other hand, the fluid behaviour is described by an Eulerian approach. A strong (two-way) coupling between the fluid and structural solutions is used because the interdependence of the fluid and structure models is important [19], [20].

The objective of this work is to assess: (i) the ability of this numerical method to model a hydrodynamic impact; (ii) the sensibility of the method to the numerical parameters; and (iii) the ability of the method to model some hydrodynamic phenomena taking place during a realistic industrial application, namely the suction. To do so, a simple test case is considered. It consists in the high-velocity and vertical impact of a wedge, based on the experiments presented in Richard [5]. Numerical results are compared to experimental results regarding hydrodynamic force and pressure measured on the structure.

This article is organised as follows. Section 2 provides a brief description of the numerical method. In Section 3, the effects of the method numerical parameters on the impact forces are discussed and the numerical and experimental results are compared. Section 4 introduces the case of the water entry and subsequent exit of a wedge. The capacity of the numerical method to model suction is thereby discussed. Finally, conclusions are drawn and orientations for future research are discussed in Section 5.

2 NUMERICAL METHOD

This section presents the method used to model the vertical impact of a wedge with the considered FE explicit solver, based on the experiments presented in Richard [5].

2.1 Structure modelling

The dimensions of the wedge are synthesised in Table 1 and corresponds to the ones described in Richard [5]. The wedge is modelled by two surfaces using 4-node shell FEs and is defined as a rigid body.

Table 1: Wedge dimensions.

Length L (mm)	Width B (mm)	Heel angle β (°)
495	320	20

2.2 Fluid modelling

The geometry of the fluid model is a rectangular parallelepiped that materializes the water and air around the structure. The air and water domains are discretised using 3D continuum 8-node FEs with 1 integration point. An Eulerian formulation is used to solve the fluid problem. The size of the fluid elements is smaller near the structure (in the impact zone) to increase the computation accuracy. The dimensions of the fluid domain are given in Fig. 1.

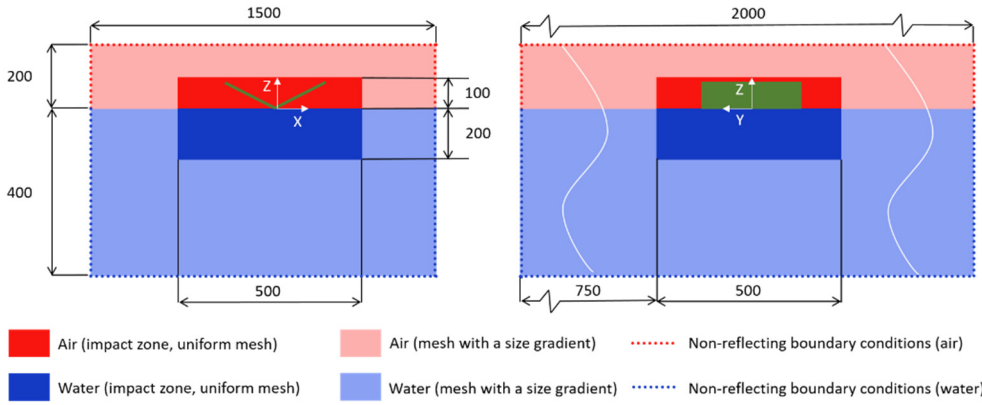

Figure 1: Dimensions of the fluid domain (in mm). Outside the impact zone, the size of the fluid elements scales with a factor 1.2. The wedge is represented in green.

2.3 Fluid–structure interaction

The fluid–structure interaction method uses structural Lagrangian elements (master), immersed in the Eulerian fluid grid (slave nodes). The structure and the fluids are meshed independently and superposed. The coupling forces are computed using a penalty method, depending on the contact height h_c and the contact stiffness k_c. The Radioss documentation suggests defining these parameters as described in eqns (1) and (2):

$$h_{c0} = 1.5 \times l_f, \tag{1}$$

$$k_{c0} = \frac{\rho U_{max}^2 S_{el}}{h_c}, \tag{2}$$

where l_f is the size of the fluid elements in contact with the structure, ρ the water density, U_{max} the structure maximum velocity and S_{el} the mean surface of the structural elements.

2.4 Initial and boundary conditions

The initial position of the lowest point of the wedge is $h_0 = 10$ mm (Fig. 2). An initial velocity $U_{max} = -10$ m/s is applied to the wedge in the $\vec{z}$ direction. Gravity acceleration is applied to all the nodes of the model (fluid and structure): $\vec{g} = -9.81.10^{-3}\vec{z}$ g/ms². The pressure in water is set at the hydrostatic pressure at the initial time step of the computation.

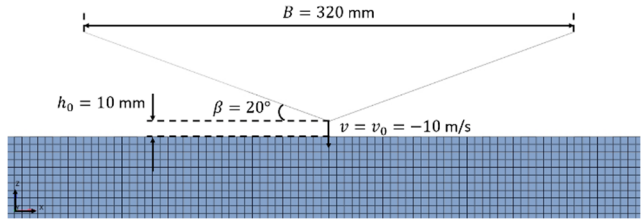

Figure 2: Initial position of the wedge above the water level.

The displacement of the mock-up is prescribed. The vertical velocity imposed to the mock-up is constant and equal to $U_{max} = -10$ m/s for the simulations presented in Section 3 and variable for the simulations presented in Section 4. Non-reflecting boundary conditions are applied on the fluid domains boundaries, based on the pressure formulation of Bayliss and Turkel [21].

3 VERTICAL AND HIGH-VELOCITY WEDGE IMPACT

Vertical wedge impact experiments have been conducted in a water tank with a high-speed shock machine as described in El Malki Alaoui et al. [22]. The tank is made of steel and is 2 m wide, 3 m long and has been filed up to 1.2 m with water during the experiments. The method used in the experiments to measure the load (hydrodynamic force, F) was based on strain gauges positioned on the piston used to move the mock-up. Pressure probes are used to measure the pressure at different locations on the wedge surface. The experimental results are presented Fig. 3 as force (slamming) and pressure coefficients (measured from a probe located on the wedge surface), obtained respectively by eqns (3) and (4).

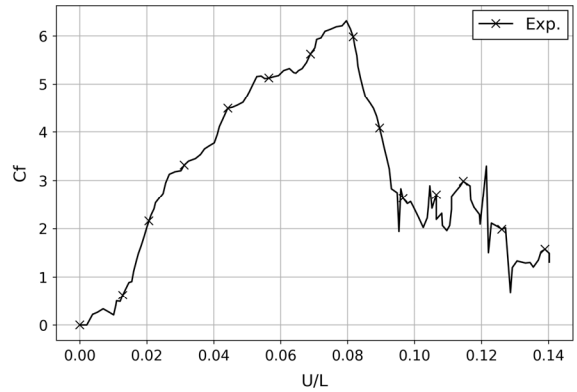

(a)

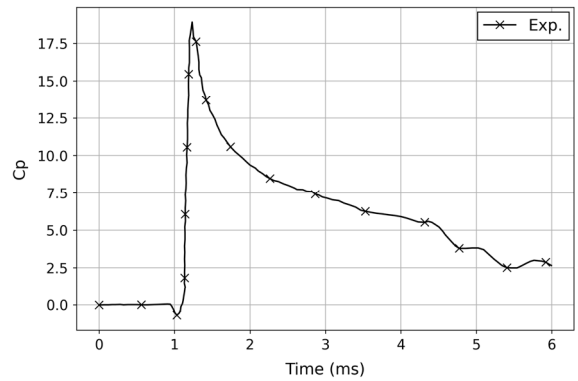

(b)

Figure 3: Experimental vertical impact of a wedge at $U_{max} = -10$ m/s. (a) Evolution of the force coefficient depending on the vertical non-dimensional displacement $\frac{U}{L}$, with U the vertical displacement of the wedge; and (b) Time-history of the pressure coefficient [5].

$$C_f = \frac{2F}{\rho_0 U_{max}^2 S}, \tag{3}$$

$$C_p = \frac{2(P-P_0)}{\rho_0 U_{max}^2}, \tag{4}$$

where F is the hydrodynamic force, P the pressure, P_0 the atmospheric pressure, U_{max} the wedge velocity and $S = L \times B$ the wedge surface projected on the xOy plane (L and B are respectively the wedge length and width).

3.1 Investigation of different numerical parameters affecting the numerical results

In this section, the effect of different numerical parameters influencing the numerical results is presented. The following points are discussed: the effect of contact stiffness and the effect of the fluid elements size in the impact zone. The conclusions drawn are then applied to the numerical model, leading to the results presented in Section 3.2.

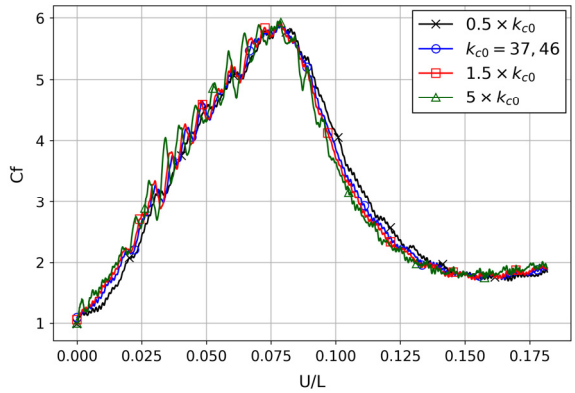

(a)

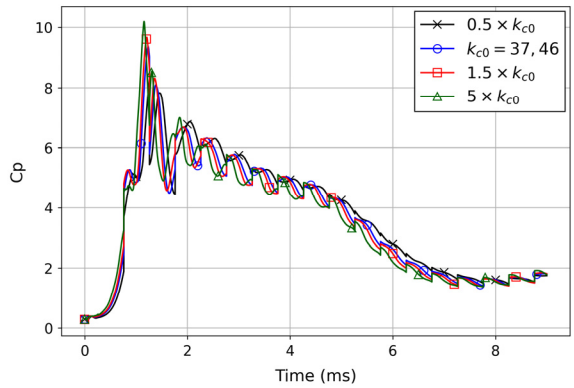

(b)

Figure 4: Numerical vertical impact of the wedge at $U_{max} = -10$ m/s for different contact stiffnesses. (a) Evolution of the force coefficient depending on the vertical non-dimensional displacement $\frac{U}{L}$, with U the vertical displacement of the wedge; and (b) Time-history of the pressure coefficient.

3.1.1 Contact stiffness

The default contact stiffness for this case is $k_{c0} = 37.46$ (see eqn (2)). The numerical results obtained for the vertical impact of a wedge for different k_c are presented in Fig. 4. The other stiffness values considered here are $k_c = 0{,}5 \times k_{c0} = 18.73$, $k_c = 1{,}5 \times k_{c0} = 56.19$ and $k_c = 5 \times k_{c0} = 187.3$.

The influence of the contact stiffness is weak considering the variations studied (factor 10 between the smallest and the largest stiffness). The maximum force coefficient remains around $C_{f\,max} \approx 5.9$ and the trends remain similar for the different contact stiffnesses studied. For a lower contact stiffness (black curve), the early response of the model diverges from the other results and the hydrodynamic force decreases more slowly after the peak. High-frequency oscillations appear in the force response when the contact stiffness increases. The amplitude of these oscillations also increases with the value of k_c (Fig. 4(a)). The local pressure measurements are similar regardless of the contact stiffness. The amplitude of the pressure peak lightly increases with k_c (Fig. 4(b)).

3.1.2 Fluid elements size

A numerical model with two symmetry plans (xOz and yOz) is used to assess the influence of the fluid elements size on the numerical results. The different elements sizes l_f investigated here range from 5 to 2 mm. The characteristics of the different models are synthesised in Table 2.

Table 2: Vertical impact of the wedge with $U_{max} = 10$ m/s. Characteristics of the models used to assess the influence of the fluid elements size l_f on the numerical results.

l_f (mm)	Total number of fluid elements	Computation time (JJ-hh:mm:ss)
5	378,736	01:11:02
4	673,171	02:43:07
3	1,399,505	11:38:31
2.5	2,202,052	22:33:42
2	3,941,772	7-09:44:14

A decrease in the elements size in the impact zone leads to a contact height decrease (see eqn (1)) and, therefore, results in a slower rise of the force coefficient in the early impact stage. With smaller elements, the force coefficient peak is larger and the force drop is slightly faster (Fig. 5(a)). The finer the mesh size, the faster is the pressure rise and the higher is the amplitude of the pressure peak (Fig. 5(b)). The numerical results globally converge with a mesh size equal to $l_f = 2.5$ mm. However, as the model uses an explicit solver, the computational cost associated with a finer mesh size is much higher.

3.2 Comparison with experimental results

The numerical results are presented for the vertical impact of the wedge. From Section 3.1 results, the fluid elements size and contact stiffness are respectively defined as $l_f = 2.5$ mm and $k_c = 74.91$. The numerical results are compared to the experimental results from Richard [5] in terms of force and pressure coefficients in Fig. 6.

The numerical model satisfyingly predicts the experimental evolution of the hydrodynamic force and pressure. The maximum force coefficient measured numerically is

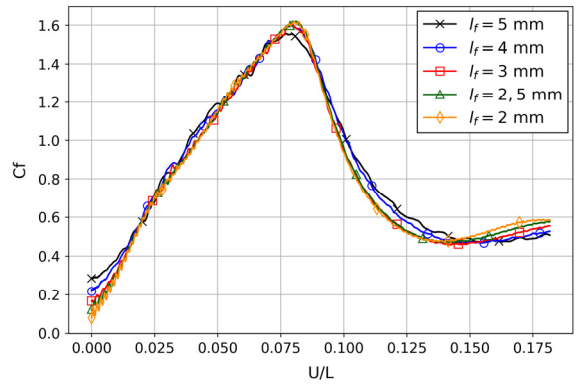

(a)

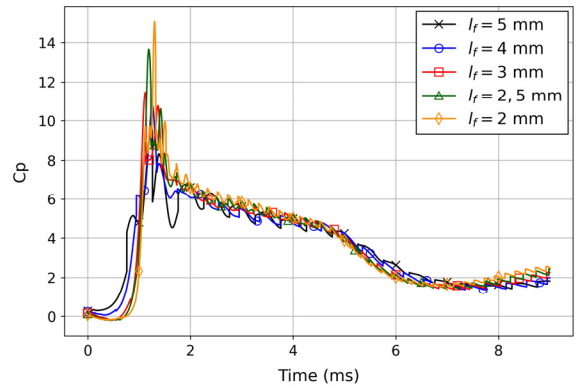

(b)

Figure 5: Numerical vertical impact of the wedge at $U_{max} = -10$ m/s for different fluid element sizes: $l_f = [2; 2.5; 3; 4; 5]$ mm. (a) Evolution of the force coefficient as a function the vertical non-dimensional displacement $\frac{U}{L}$, with U the vertical displacement of the wedge; and (b) Time-history of the pressure coefficient.

similar to the experimental one (difference inferior to 1%). However, at the first instants of the simulation, the numerical model overestimates the hydrodynamic force level. The numerical model underestimates the decrease of the force coefficient after the force peak.

The pressure rise occurs earlier in the numerical simulation than in the experiments. Also, the numerical model underestimates the pressure coefficient peak and general level of pressure.

Some discrepancies between the numerical and experimental results can be explained by the numerical method used in the present work. Indeed, fluid–structure interaction forces appear when a fluid node is detected within the contact height of the structure. The results at the first instants of the simulation are related to the detection of fluid nodes within the contact height of the structure, before the physical contact between the wedge and the water.

There are some discrepancies between the numerical and experimental pressure evolutions. Numerically the pressure is measured at a normal distance from the wedge surface

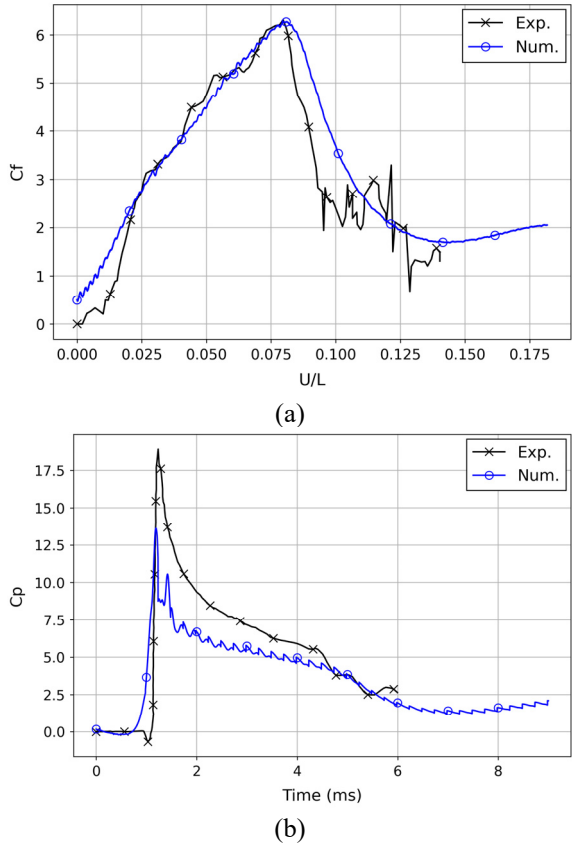

Figure 6: Comparison of the experimental [5] and numerical results for the vertical impact of the wedge at $U_{max} = -10$ m/s. (a) Evolution of the force coefficient as a function of the vertical non-dimensional displacement $\frac{U}{L}$, with U the vertical displacement of the wedge; and (b) Time-history of the pressure coefficient.

slightly larger than the contact height ($dist = \frac{4}{3}h_{c0}$), as illustrated in Fig. 8. Experimentally the pressure probe is located on the wedge surface. The pressure peak is a spatially and temporally localised phenomenon. This explains why the present numerical method underestimates the pressure levels.

4 HIGH-VELOCITY WATER ENTRY AND SUBSEQUENT EXIT OF A WEDGE

In this section, the present numerical method is applied to the high-velocity water entry and subsequent exit of a wedge. The numerical model is similar to the one considered in Section 3.2, but the velocity prescribed to the wedge is now given by eqn (5), following the method used by Breton et al. [23] to experimentally study suction at lower velocities:

$$U = U_{max}\cos(\omega t + \Phi), \tag{5}$$

where U_{max} is the maximum velocity of the wedge, ω the pulsation, t the time and Φ the phase defined to ensure a variation of U from $-U_{max}$ to U_{max} during the simulation. For the

present simulation, the following values of the parameters have been adopted: $U_{max} = 10$ m/s, $\omega = \frac{\pi}{T}$, $T = 15$ ms and $\Phi = \pi$.

The numerical results in terms of hydrodynamic force and pressure are presented in Fig. 7(a) and 7(b), respectively. The hydrodynamic force increases until a maximum value is reached (positive force peak). Then, the force decreases and becomes negative (suction force) as the wedge decelerates. The force reaches a minimum value at the transition between the entry and exit stages, i.e. when the penetration depth reaches its maximum and the velocity of the wedge is null. After, the force gradually returns to 0. The amplitude of the negative force peak is more than 3 times higher than the positive force peak.

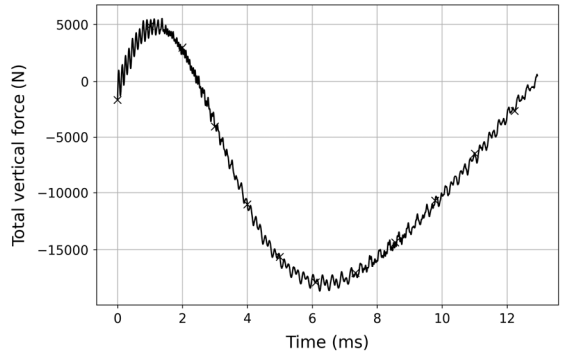

(a)

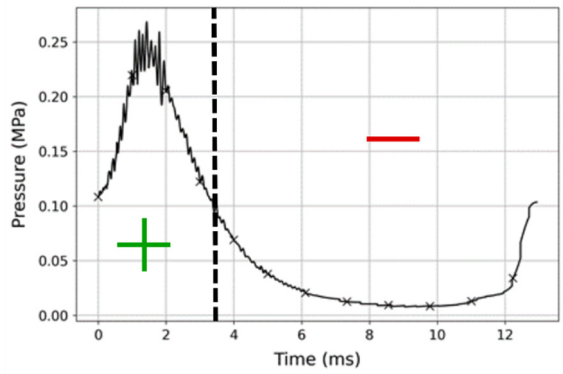

(b)

Figure 7: Numerical entry and subsequent exit of the wedge with $U_{max} = 10$ m/s. (a) Time history of the hydrodynamic force; (b) Time-history of the pressure. The probe location is illustrated in Fig. 8. The dashed line separates the stages where the pressure is positive and negative, relatively to $P = 0.1$ MPA.

A pressure peak is measured at the first instants of the simulation, when the water reaches the probe. The probe location is illustrated in Fig. 8. Then, as the penetration depth of the wedge increases and its velocity decreases, the pressure decreases. Around $t = 3.5$ ms, the pressure becomes lower than the ambient pressure ($P_0 = 0.1$ MPa), indicating the occurrence of suction forces, and stabilises around $P \approx 0.008$ MPa. From $t = 10$ ms, the pressure gradually increases to $P = 0.1$ MPA (the ambient pressure). The increase of the pressure

corresponds to the opening of the cavity formed under the wedge (ventilation) during the impact (Fig. 8).

The numerical model is able to simulate a negative force and (relative) pressure experienced by the structure at the transition between the entry and exit stages. As the velocity is high, the wedge also experiences a detachment of the fluid (water) and a cavity is formed under the wedge.

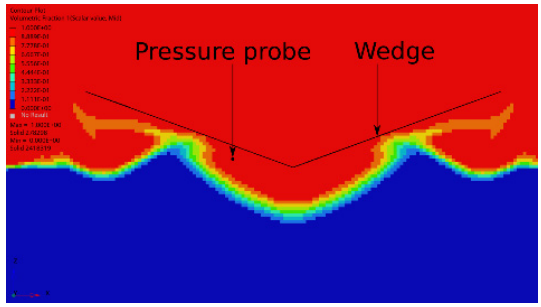

Figure 8: Numerical entry and subsequent exit of the wedge with $U_{max} = 10$ m/s. The figure shows the air volume fraction at $t = 11$ ms. The opening of a cavity under the wedge is visible (ventilation).

5 CONCLUSIONS AND DISCUSSION

In the present article, the numerical simulation of the water entry and water entry and subsequent exit of a wedge have been analysed. The hydrodynamic force and pressure evolutions are emphasised. The study has been carried out numerically using an explicit FE solver (*Radioss*) and a CEL approach.

The numerical results have been compared with existing experimental results for the water entry case. A fairly good agreement has been observed. This study assessed the influence of the most influential numerical parameters on the simulation results. First, varying the contact stiffness has little influence on the numerical hydrodynamic force and pressure evolutions. Second, for the considered element sizes, smaller elements lead to more precise numerical results, but to much higher computation times. The element size also influences the contact stiffness. Therefore, it is a key parameter when modelling hydrodynamic impacts using the present numerical method.

The model also showed its capability to model negative (suction) force and relative pressure. The higher amplitude of the negative force peak further justifies the interest of studying suction phenomena during hydrodynamic impacts representative of realistic industrial applications. However, the numerical model requires validation against experimental results. Therefore, future work will be dedicated to the simulation of experimental cases involving suction forces.

ACKNOWLEDGEMENT

The authors are grateful to ONERA and IFREMER for co-funding this project.

REFERENCES

[1] von Karman, T., The impact on seaplane floats during landing. Report 321, NACA, Aerodynamical Institute of the Technical High School, Aachen, Oct. 1929. Number: NACA-TN-321.

[2] Wagner, H., Phenomena associated with impacts and sliding on liquid surfaces. Technical report. Translation of Über StoB und Gleitvorgänge an der Oberfläche von Flüssigkeiten. *Z. Angew. Math. Mech.*, **12**, pp. 193–215, 1932.
[3] Greenhow, M., Wedge entry into initially calm water. *Applied Ocean Research*, **9**, pp. 214–223, 1987.
[4] Russo, S., Jalalisendi, M., Falcucci, G. & Porfiri, M., Experimental characterization of oblique and asymmetric water entry. *Experimental Thermal and Fluid Science*, **92**, pp. 141–161, 2018.
[5] Richard, Y., Etudes numériques et expérimentales des impacts hydrodynamiques primaires et secondaires lors du tossage de sections de carènes, Doctoral thesis, ENSTA Bretagne, 2021.
[6] Cointe, R. & Armand, J.-L., Hydrodynamic impact analysis of a cylinder. *Journal of Offshore Mechanics and Arctic Engineering*, **109**, pp. 237–243, 1987.
[7] Campbell, I.M.C. & Weynberg, P., Measurement of parameters affecting slamming. Wolfson Unit for Marine Technology and Industrial Aerodynamics, University of Southampton, Report, vol. no. 440, 1980.
[8] Baldwin, J.L., Vertical water entry of cones. Technical report, Naval Ordnance Laboratory, White Oak, MD, Feb. 1971.
[9] Mai, T., Greaves, D. & Raby, A., Aeration effects on impact: drop test of a flat plate. *The 24th International Ocean and Polar Engineering Conference*, Busan, Korea, p. 7, 2014.
[10] Baldwin, J.L. & Steves, H.K., Vertical water entry of spheres. Technical report, Naval Surface Weapons Center, White Oak Laboratory, Silver Spring, MD, May 1975.
[11] Ribet, H., Laborde, P. & Mahé, M., Numerical modeling of the impact on water of a flexible structure by explicit finite element method: Comparisons with *Radioss* numerical results and experiments. *Aerospace Science and Technology*, **3**, pp. 83–91, 1999.
[12] Jacques, N., Constantinescu, A., Kerampran, S. & Nême, A., Comparaison de différentes approaches pour la simulation numérique d'impacts hydrodynamiques. *European Journal of Computational Mechanics*, **19**, pp. 743–770, 2010.
[13] Anghileri, M., Castelletti, L.-M.L., Francesconi, E., Milanese, A. & Pittofrati, M., Survey of numerical approaches to analyse the behavior of a composite skin panel during a water impact. *International Journal of Impact Engineering*, **63**, pp. 43–51, 2014.
[14] Piro, D.J. & Maki, K.J., Hydroelastic analysis of bodies that enter and exit water. *Journal of Fluids and Structures*, **37**, pp. 134–150, 2013.
[15] Pentecôte, N. & Vigliotti, A., Crashworthiness of helicopters on water: Test and simulation of a full-scale WG30 impacting on water. *International Journal of Crashworthiness*, **8**, pp. 559–572, 2003. DOI: 10.1533/ijcr.2003.0259.
[16] Siemann, M.H. & Langrand, B., Coupled fluid-structure computational methods for aircraft ditching simulations: Comparison of ALE-FE and SPH-FE approaches. *Computers and Structures*, **188**, pp. 95–108, 2017.
[17] Delsart, D., Langrand, B. & Vagnot, A., Evaluation of a Euler/Lagrange coupling method for the ditching simulation of helicopter structures. *5th International Conference on Fluid Structure Interaction*, **105**, Royal Mare Village, Crete, Greece, May, 2009.
[18] Ortiz, R., Portemont, G., Charles, J. & Sobry, J., Assessment of explicit FE capabilities for full scale coupled fluid/structure aircraft ditching simulations. *23rd International Congress of the Aeronautical Sciences*, Jan., 2002.

[19] Souli, M. & Sigrist, J.-F., *Interaction Fluide–Structure: Modélisation et Simulation Numérique*, vol. 19, Hermès – Lavoisier, 2010.
[20] Casadei, F., Leconte, N. & Larcher, M., Strong and weak forms of a fully non-conforming FSI algorithm in fast transient dynamics for blast loading of structures. *EU Science Hub – European Commission*, Corfu, Greece, Nov., p. 20, 2011.
[21] Bayliss, A. & Turkel, E., Out flow boundary conditions for fluid dynamics. *SIAM Journal on Scientific and Statistical Computing*, **3**(2), 1982. DOI: 10.1137/0903016.
[22] El Malki Alaoui, A., Nême, A., Tassin, A. & Jacques, N., Experimental study of coefficients during vertical water entry of axisymmetric rigid shapes at constant speeds. *Applied Ocean Research*, **37**, pp. 183–197, 2012.
[23] Breton, T., Tassin, A. & Jacques, N., Experimental investigation of the water entry and/or exit of axisymmetric bodies. *Journal of Fluid Mechanics*, **901**, A37, 2020. DOI: 10.1017/jfm.2020.559.